

Light scattering from self-affine fractal silver surfaces with nanoscale cutoff: Far-field and near-field calculations

José A. Sánchez-Gil* and José V. García-Ramos

Instituto de Estructura de la Materia, Consejo Superior de Investigaciones Científicas, Serrano 121, E-28006 Madrid, Spain

Eugenio R. Méndez

División de Física Aplicada,

Centro de Investigación Científica y de Educación Superior de Ensenada

Ensenada, Baja California 22800, México

(Dated: October 30, 2018)

We study the light scattered from randomly rough, one-dimensional self-affine fractal silver surfaces with nanoscale lower cutoff, illuminated by s - or p -polarized Gaussian beams a few microns wide. By means of rigorous numerical calculations based on the Green theorem integral equation formulation, we obtain both the far- and near-field scattered intensities. The influence of diminishing the fractal lower scale cutoff (from below a hundred, down to a few nanometers) is analyzed in the case of both single realizations and ensemble average magnitudes. For s polarization, variations are small in the far field, being only significant in the higher spatial frequency components of evanescent character in the near field. In the case of p polarization, however, the nanoscale cutoff has remarkable effects stemming from the roughness-induced excitation of surface-plasmon polaritons. In the far field, the effect is noticed both in the speckle pattern variation and in the decrease of the total reflected energy upon ensemble averaging, due to increased absorption. In the near field, more efficient excitation of localized optical modes is achieved with smaller cutoff, which in turn leads to huge surface electric field enhancements.

PACS numbers: 290.5880, 290.4210, 240.6680, 180.5810.

I. INTRODUCTION

Since the early days of fractality,[1] the scattering of electromagnetic (EM) waves from fractal surfaces has been a field of intense activity. Physical fractals appear ubiquitously in nature, possessing fractal properties within a broad, however finite, range of scales. Therefore the study of classical wave scattering from fractals is a problem of interest not only from a fundamental point of view, but also from the practical knowledge that probing technologies such as surface optical characterization, remote sensing, radar, sonar, etc. can yield about a wide variety of systems. In fact, it is now well understood that many naturally occurring surfaces exhibit scale invariance, particularly in the form of self-affinity.[1, 2, 3]

There exists a large amount of theoretical works devoted to wave scattering from fractal surfaces.[4, 5, 6, 7, 8, 9, 10, 11, 12, 13, 14, 15, 16, 17, 18, 19, 20, 21, 22] Most of them make use of approximations, such as Kirchhoff approximation (KA) or perturbation methods, in order to obtain analytical expressions that are useful in certain regimes, but thereby imposing a constraint on the length scales over which fractality might be present. Others include calculations within the Rayleigh hypothesis and/or restricted to perfectly conducting surfaces. And only very recent works are capable of dealing with arbi-

trarily rough metal or dielectric surfaces,[17, 18, 21, 22] on the basis on the Green's theorem integral equation formulation for rough surface scattering.[23, 24, 25]

On the other hand, in addition to far field scattering, the near EM field on self-affine fractals has attracted a great deal of attention.[26, 27, 28, 29, 30, 31, 32] To a large extent, the interest lies in the observation in the near field intensity distributions, through photon scanning tunneling microscopy (PSTM), of large concentrations of EM field intensity on *bright spots*.[31, 33, 34, 35, 36, 37, 38] The appearance of such *localized optical modes* is mediated by the roughness-induced excitation of surface-plasmon polaritons (SPP) on very rough surfaces with subwavelength features. The occurrence of large surface EM fields is indeed crucial to the EM mechanism in Surface-Enhanced Raman Scattering (SERS) and to other non-linear surface optical processes.[26, 29, 30, 31, 32, 38, 39] Furthermore, the predicted, enormously high values of the surface electric field intensity have been related to the recent observation of SERS single molecule probing.[40, 41, 42]

It is our aim to employ the above mentioned rigorous Green's theorem formulation to study the far-field and near-field scattered from one-dimensionally rough, self-affine fractal Ag surfaces, restricted to one dimension for the sake of computational limitations. The scattering model is described in Sec. II. We focus on fractals preserving self-affinity from tens of microns to subwavelength dimensions. Actually, we analyze the influence of the lower scale cutoff as is reduced from ~ 100 nm (as used in Refs. 17, 18, 28, 29, 32) to a few nanometers. It

*Electronic address: j.sanchez@iem.cfmac.csic.es; URL: http://www.iem.cfmac.csic.es/departamentos/espvib_procmult/jjsanchez.htm

should be mentioned that the effect on the far field of the lower scale cutoff in deterministic Koch fractals has been previously studied.[17] The results for the far-field and near-field calculations are presented in Secs. III and IV, respectively. Finally, the main conclusions derived from this work are summarized in Sec. V.

II. SCATTERING MODEL

The scattering geometry is depicted in Fig. 1. A monochromatic, linearly polarized Gaussian beam of frequency ω and $1/e$ amplitude half width W impinges at an angle θ_0 on a randomly rough surface $z = \zeta(x)$. The rough interface separates vacuum from a semi-infinite silver volume occupying the lower half-space [$z < \zeta(x)$] and characterized by an isotropic, frequency-dependent homogeneous dielectric function $\epsilon(\omega)$.

With the aim of solving this scattering problem for arbitrarily large roughness parameters, we make use of the scattering integral equations based on the application of Green's second integral theorem.[24] It is well known that this full vectorial formulation is considerably simplified when restricted to 1D surfaces and linear polarization, thereby being reduced to four scalar integral equations for the only nonzero component of either the electric field amplitude

$$\mathbf{E}^{(s)} \equiv E^{(s)}(\mathbf{r}, \omega) \hat{\mathbf{y}},$$

with

$$\mathbf{H}^{(s)} \equiv H_x^{(s)}(\mathbf{r}, \omega) \hat{\mathbf{x}} + H_z^{(s)}(\mathbf{r}, \omega) \hat{\mathbf{z}},$$

for s polarization, or the magnetic field amplitude

$$\mathbf{H}^{(p)} \equiv H^{(p)}(\mathbf{r}, \omega) \hat{\mathbf{y}},$$

with

$$\mathbf{E}^{(p)} \equiv E_x^{(p)}(\mathbf{r}, \omega) \hat{\mathbf{x}} + E_z^{(p)}(\mathbf{r}, \omega) \hat{\mathbf{z}},$$

for p polarization.[23, 25] Two of these surface integral equations can be used as extended boundary conditions, which (recalling the continuity relations across the interface) lead to a system of two coupled integral equations for the surface field and its normal derivative. This can be solved numerically in the form of linear equations by means of a quadrature scheme.[23, 25] Once these source functions are obtained, it is straightforward to calculate the far field scattered intensity,[25] and in general the electric (magnetic) field amplitude for s (p) polarization at any point in vacuum or inside the metal from two of the integral equations.[29] In addition, from the latter integral equations, the corresponding expressions for the magnetic (electric) field amplitudes for s (p) polarization can be simply obtained by making use of Maxwell equations (cf. Ref. 32 in the case of p polarization). These expressions can be useful in near electric or magnetic

field calculations. However, they exhibit non-integrable singularities when approaching the surface profile.

In this regard, the calculation of the surface magnetic field intensity for s polarization has been done in a simple manner by exploiting the connection between its normal and tangential components on the vacuum side

$$H_n^{(s)}(x) = -\frac{ic}{\omega} \gamma^{-1} \frac{dE^{(s)}(x)}{dx}, \quad (1a)$$

$$H_t^{(s)}(x) = \frac{ic}{\omega} \gamma^{-1} F^{(s)}(x), \quad (1b)$$

with the surface electric field and its normal derivative from the vacuum side,

$$E^{(s)}(x) = E^{(s,>)}(x, \zeta(x)), \quad (2a)$$

$$F^{(s)}(x) = \gamma \left. \frac{\partial E^{(s,>)}(\mathbf{r})}{\partial n} \right|_{z=\zeta^{(+)}(x)}, \quad (2b)$$

with $\gamma \equiv [1 + [\zeta'(x)]^2]^{1/2}$. The corresponding expressions for the surface electric field components for p polarization are given by:[32]

$$E_n^{(p)}(x) = \frac{ic}{\omega} \gamma^{-1} \frac{dH^{(p)}(x)}{dx}, \quad (3a)$$

$$E_t^{(p)}(x) = -\frac{ic}{\omega} \gamma^{-1} L^{(p)}(x), \quad (3b)$$

where

$$H^{(p)}(x) = H^{(p,>)}(x, \zeta(x)) \quad (4a)$$

$$L^{(p)}(x) = \gamma \left. \frac{\partial H^{(p,>)}(\mathbf{r})}{\partial n} \right|_{z=\zeta^{(+)}(x)}. \quad (4b)$$

As mentioned above, $E^{(s)}(x)$, $F^{(s)}(x)$, $H^{(p)}(x)$, $L^{(p)}(x)$ constitute the source functions of the integral equations in this scattering configuration.

As a model describing many naturally occurring surface growth phenomena exhibiting self-affine fractality, we have chosen that given by the trace of a fractional Brownian motion through Voss' algorithm,[2, 43, 44] In addition, this model yields self-affine fractal structures that resemble fairly well the properties of some SERS metal substrates.[35, 36, 38] The ensembles of realizations thus generated are characterized by their fractal dimension $D = 2 - \mathcal{H}$ (\mathcal{H} being the Hurst exponent) and rms height δ . (In order to avoid the inherent ambiguity in the definition of the rms height for self-affine fractals, δ refers in our calculations to the rms height defined over the entire fractal profile with length $L_f = 51.4 \mu\text{m}$. Recall that δ depends on the length Δx over which it is measured through[22] $\delta = l^{1-\mathcal{H}} \Delta x^{\mathcal{H}}$, l being the topothesy. Thus the topothesy l will be also given. From each generated fractal profile with N_f points and length L_f , sequences of N points (with constant N/N_f) are extracted to obtain similar profiles with identical properties except for the lower scale cutoff as determined by $\xi_L = L_f/N_f$. (Strictly speaking, ξ_L should be given by the minimum

length scale above which the ensemble of such realizations exhibit self-affinity, resulting in a value typically larger than the mere discretization cutoff.[2, 29])

From now on, we will focus below on the fractal dimension $D = 1.9$. This choice is justified for we expect the influence of decreasing ξ_L to be more significant for larger fractal dimensions. And recall that the effect of varying D has been already studied on the far field [18] and the near field [29], albeit for a relatively large lower cutoff ξ_L . The values of the lower scale cutoffs hitherto considered are $\xi_L = 51.4, 25.7, 12.85$, and 6.425 nm, resulting from sequences of $N = 102, 205, 410$, and 819 points extracted from profiles with $N_f = 1024, 2048, 4096$, and 8192 points. The length of all realizations is thus $L = L_f(N/N_f) = 5.14 \mu\text{m}$. Actually, the final number of sampling points per realization used in the numerical calculations is significantly higher for the sake of accuracy: $N_p = n_i N$ as obtained by introducing $n_i = 4-10$ cubic-splined interpolating points, the latter being chosen on the basis of numerical convergence tests.

III. FAR FIELD

First, we present in Fig. 2 the angular distributions of the speckle pattern intensities scattered from self-affine Ag surface profiles with identical properties ($D = 1.9$, $L = 5.14 \mu\text{m}$, and δ) except for $\xi_L = 51.4, 25.7, 12.85$, and 6.425 nm, as mentioned in the preceding section. Both s - and p -polarized incident ($\theta_0 = -10^\circ$) Gaussian beams are considered with wavelength $\lambda = 2\pi c/\omega = 629.9$ nm and $W = (L/4) \cos \theta_0$, the dielectric constant of Ag at this frequency being[45] $\epsilon = -15 + i$. The upper plots correspond to moderately rough surfaces with $\delta = 51.4$ nm and topography $l = 24$ nm (the corresponding surface profiles will be shown in Fig. 5d), beyond the reach of standard approximate treatments such as the KA or perturbation theories. No significant differences are found (note the semi-log scale in order to enhance them) for s polarization, nor even away from the bright specular peak. In the case of p polarization, a weak decrease in the specular peak with decreasing ξ_L is barely observed, whereas small differences appear in the speckle pattern away from the specular peak.

We now consider rougher surfaces with $\delta = 257$ nm and topography $l = 143$ nm (see Figs. 2c and 2d). Appreciable changes are observed in the s -polarized speckle with decreasing ξ_L , although the patterns are qualitatively similar. However, in the case of p -polarized speckle patterns, differences are both quantitative and qualitatively notorious. Note the absence of specular peaks in both polarizations. Therefore, in light of Figs. 2a and 2d, it is seen that the details at nanometer scales produce no change in the s -polarized speckle patterns for moderately rough self-affine profiles, appearing only small quantitative variations for very large rms height. For p polarization, nonetheless, small changes are already observed for moderately rough profiles, becoming dramatic for large

roughness.

Next, the influence of nanoscales on the mean scattered intensities is analyzed. This is done in Figs. 3 after averaging speckle pattern distributions over an ensemble of $N_{rea} = 200$ realizations. Experimentally, this can be achieved either by also ensemble averaging, or by illuminating a very large surface and collecting a large amount of speckles at every scattering angle (or a combination of both). In the case of the self-affine fractals with $\delta = 51.4$ nm (see Figs. 3a and 3b), the diffuse component of the mean scattered intensity in s polarization is not altered at all with decreasing lower scale cutoff. As for the specular, which amounts to $\sim 32\%$, and not shown in Fig. 3a), the same is true. The p -polarized diffuse component in Fig. 3b shows no significant variation at angles away from the specular direction, whereas a very small, but observable, decrease in the specular direction is observed when the lower scale cutoff diminishes. On the other hand, the p -polarized specular component, not shown in Fig. 3b, exhibits a larger decrement (from $\sim 32\%$ down to $\sim 24\%$) with diminishing ξ_L . Interestingly, despite the specular components are not included in Figs. 3a and 3b, the resulting angular distributions of diffusely scattered intensities present pronounced peaks at the specular directions. These diffuse specular peaks have been already discussed in Ref. 18 for self-affine fractals with various fractal dimensions but a higher lower scale cutoff; the results in Figs. 3a and 3b demonstrate that such peaks are not substantially affected by the fractal scales below a hundred nanometers.

Ensemble averaging of the speckle pattern scattered from very rough ($\delta = 257$ nm) self-affine fractal surfaces also tends to wash out differences arising from nanoscale fractal details (see Figs. 3c and 3d). In fact, no differences are found in the angular distribution of s -polarized, mean scattered intensities (leaving aside some spurious speckle noise due to the limited number of realizations employed), even though quantitative changes have been found above in the speckle patterns for single realizations (see Fig. 2c). Furthermore, the remarkable qualitative and quantitative changes in the p -polarized speckle spots seen in Fig. 2d reduce to significant, though only quantitative, variations upon ensemble averaging as shown in Fig. 3d. And if the effect of absorption, defined as $A = 1 - S$ (S being the normalized reflectance) is taken into account, the resulting renormalized angular distributions of p -polarized mean scattered intensities, $\langle I(\theta) \rangle / S$, exhibit little differences with decreasing fractal lower scale cutoff (see Fig. 4). Incidentally, note that the remaining speckle noise in Figs. 3d and 4 hinders the possible observation of a backscattering peak due to the multiple scattering of SPP.[18]

IV. NEAR FIELD

We now turn to the investigation of the influence on the near EM field of the lower scale cutoffs of the self-affine

fractal surfaces whose far-field scattering properties have been studied in the preceding section. Near field intensity distributions are relevant for the information they provide on the scattering process, and can be measured through near-field optical microscopy.

First, we calculate the intensities of all the EM field components on the surface. The results for the moderately rough fractals with $\delta = 51.4$ nm employed in the speckle pattern calculations in Fig. 2 are shown in Figs. 5 and 6 for s and p polarization, respectively. The corresponding surface profiles are shown in the bottom, Figs. 5d and Figs. 6d. The nonzero components of the EM field being plotted are (cf. Sec. II): the tangential, perpendicular to the incident plane, electric (respectively, magnetic) field and the normal and tangential (in the plane of incidence) magnetic (respectively, electric) field, in the case of s (respectively, p) polarization. For the sake of clarity, only the central part of the illuminated surface is shown.

Before analyzing the spatial distributions, let us recall what is expected within the KA, namely, the sum of the incident and the specularly (locally) reflected fields. Since the angular variation of the Fresnel coefficients for metals at this frequency is small, the local variations of the specular field can be neglected. Therefore, the KA field intensities are approximately given by those for a planar surface, namely:

$$|E^{(s,KA)}|^2 \approx |1 + \mathcal{R}_s|^2 |E^{(s,i)}|^2 \quad (5a)$$

$$|H_n^{(s,KA)}|^2 \approx \sin^2 \theta_0 |1 + \mathcal{R}_s|^2 |H^{(s,i)}| \quad (5b)$$

$$|H_t^{(s,KA)}|^2 \approx \cos^2 \theta_0 |1 - \mathcal{R}_s|^2 |H^{(s,i)}|, \quad (5c)$$

for s polarization; and

$$|H^{(p,KA)}|^2 \approx |1 + \mathcal{R}_p|^2 |H^{(p,i)}|^2 \quad (6a)$$

$$|E_n^{(p,KA)}|^2 \approx \sin^2 \theta_0 |1 + \mathcal{R}_p|^2 |E^{(p,i)}| \quad (6b)$$

$$|E_t^{(p,KA)}|^2 \approx \cos^2 \theta_0 |1 - \mathcal{R}_p|^2 |E^{(p,i)}|, \quad (6c)$$

for p polarization, \mathcal{R}_s and \mathcal{R}_p being the corresponding Fresnel coefficients for θ_0 on a planar metal surface. The latter field intensities are plotted in Figs. 5 and 6. As expected, the KA does not hold even for the moderately rough surface profiles used therein, nor does perturbation theory (recall that the planar surface field intensities can be considered the zeroth order approximation in the small-amplitude perturbation expansion of the field), but they provide the background about which the actual surface EM field intensities strongly vary.

In the case of s polarization, Fig. 5, significant variations appear in the surface EM field upon decreasing the lower scale cutoff. No appreciable differences have been found in the corresponding far field speckle patterns in Fig. 2a and 2b, so that the surface field nanoscale fluctuations are mostly due to the evanescent components. Fluctuations about the background distributions, Eqs. (5), become narrower and steeper the smaller is ξ_L , namely, the smaller are the surface features. This

effect is more pronounced for the normal magnetic field, for which the expected KA background is indeed very small. Interestingly, it should be noted that the electric field intensity resembles with positive contrast the surface profile (the same is true for the total, tangential plus normal, magnetic field intensity), which is not the case in general.[46] Although not valid from a quantitative standpoint, small amplitude perturbation theory can provide a qualitative explanation. The first-order term of the surface electric field in powers of the surface height, which in turn gives the first-order correction to the planar surface background,[46, 47] can be cast for this particular scattering geometry, polarization and near normal incidence in the form of a convolution integral involving the surface profile function. We have verified, though not shown here, that by simply increasing the angle of incidence up to $\theta_0 = 40^\circ$ the resemblance is slightly lost.

Upon illuminating with p -polarized light, see Fig. 6, the surface EM field intensity distributions become more complicated, with larger variations from one realization to another with diminishing ξ_L , and no resemblance whatsoever with the surface profiles. These variations are considerably larger than those for the far-field speckle patterns, indicating the crucial role played by the evanescent components. Furthermore, the excitation of SPP propagating along the surface and reradiating into vacuum mediates the scattering process. In fact, the spatial frequency of the large oscillations about the background in the surface EM field intensity is related to the SPP wavelength:[29] this is more easily observed in the surface magnetic field in Fig. 6a (also in the total electric field, not shown here) for the profiles with higher ξ_L . On the other hand, the surface normal electric field component for the smaller ξ_L (see Fig. 6b) reveals the appearance of narrow and bright spots where an enhancement of the field intensity of nearly two orders of magnitude occur, despite the relatively low value of δ . This clearly manifests the crucial role played by the lower scale cutoff in the excitation of localized optical modes.[48]

What if the surface roughness parameter is increased? In Figs. 7 and 8, the surface EM field intensities are plotted for s and p polarization, respectively, as in Figs. 5 and 6, but for $\delta = 257$ nm. Due to the large differences introduced by ξ_L , a semi-log scale is used and only a small surface region about one wavelength long is shown. In the case of s polarization, the differences in the surface EM field intensities from one realization to another with lower ξ_L are remarkable, and quantitatively larger than those differences shown above for smoother surface profiles; the qualitative behavior is however similar. Lower- ξ_L surfaces lead to surface EM field intensities with higher spatial frequency components, but the smoothly varying envelopes corresponding to smaller spatial frequencies are largely preserved. The former are mostly evanescent components that contribute little to the far-field intensities, which are basically originated in the propagating components, and thus quite similar for all surface profiles (see Fig. 2c). It should be remarked

that no localized optical excitations seem to appear, as expected since no SPP can be excited, nor significant EM field enhancements are found. Note that, thanks to the semi-logarithmic scale used in Figs. 7 for the surface field intensities, a weak qualitative resemblance of positive contrast with the surface profiles can be seen.

The p -polarized surface EM field intensities presented in Fig. 8 reveal very strong changes in all field components with lower ξ_L . These changes are considerably stronger than those for the smoother surfaces (see Fig. 6). As mentioned above, narrow, large peaks tend to concentrate at bright spots in the form of *localized optical modes*, exhibiting very large electric field enhancements preferentially polarized along the normal to the surface, in agreement with the SPP polarization, although significantly large enhancements of the tangential electric field intensity are also found. In addition, large magnetic field intensities abound, not necessarily at the same electric field bright spots. The polarization of the modes has been discussed in Ref. 32 for rougher self-affine fractals with large, but yet subwavelength, ξ_L . It should be emphasized that the nanoscale lower cutoff largely contributes to the building and strengthening of such optical excitations.

Let us plot the EM field in the near vicinity of the rough interface. This is done in Figs. 9 and 10, where the near-field intensity maps in a logarithmic scale for s and p polarization, respectively, are shown in a region around the origin of the surface profile with $\xi_L = 12.85$ nm in Figs. 7d and 8d. All the EM field components are included for the sake of completeness; recall that it has been recently reported that the magnetic field intensity can be also probed through PSTM for certain experimental configurations.[49] The actual surface profile, though not explicitly depicted, can be inferred from the fairly black, metal regions due to the evanescent behavior of the EM fields inside metal with a small skin depth ($d \approx 25$ nm).

Note that no bright spot whatsoever is observed in the EM field intensity maps in the case of s polarization, Fig. 9, which exhibits no relevant features in the near field. The actual interface appears slightly blurred, since the minima have been reduced to enhance contrast. Incidentally, the continuity of the (tangential) electric field is satisfied in Fig. 9a, as well as the (dis)continuity of the (normal) tangential magnetic field in Figs. 9c and 9d.

On the other hand, a very bright spot is found at the local maximum in the central part of the intensity map in Fig. 10a: The intensity field enhancement at such spot is $|E|^2 / |E^{(i)}|^2 \sim 10^4$ (recall that the maximum scale of EM field intensities in Fig. 9 is about 3 orders of magnitude lower than those in Fig. 10). Note that there seems to be a bright, though weaker, magnetic spot associated with the optical mode (see Fig. 10b), which is nonetheless slightly shifted to the right of the electric field maximum, on the surface local minimum nearby. The electric field intensity decays rapidly upon moving into vacuum away from the bright spot, faster than expected for the evanes-

cent decay of SPP propagating on a plane. This may help to explain why localized optical modes experimentally observed through PSTM yield considerably smaller enhancement factors,[37] leaving aside the fact that no direct comparison with theoretical calculations for the actual experimental surface profile are available. With regard to the electric field orientation on the bright spot, Figs. 10c and 10d indicate that the normal electric field component is responsible for the bright spot, in agreement with Figs. 8b and 8c; this component corresponds to $|E_z|^2$ in regions near surface maxima and minima (see Fig. 10d) and to $|E_x|^2$ near vertical surface walls (see Fig. 10c). It can be also observed that, as expected, the normal electric field is discontinuous across the interface, the tangential component being continuous. The continuity of the (tangential) magnetic field for p polarization is evident in Fig. 10a.

The statistics of the surface electric field enhancement has been studied elsewhere,[48] confirming a significant increase with decreasing ξ_L . It should be remarked that such large surface electric fields plays a decisive role in SERS and other surface non-linear optical processes;[26, 29, 39] in particular, local values of $\sim 10^4$ can help to explain the existence of bright spots at which SERS single-molecule detection has been claimed.[40, 41, 42]

V. CONCLUDING REMARKS

To summarize, we have studied the influence of the nanoscale (in the region below a hundred nanometers) lower cutoff ξ_L on the scattering of light from one-dimensional, self-affine fractal Ag surfaces with large fractal dimension $D = 1.9$ and for both moderately ($\delta = 51.45$ nm) and large ($\delta = 257$ nm) surface height deviations. Since no approximate methods are applicable for such roughness parameters, numerical calculations have been carried out on the basis of the Green's theorem integral equation formulations, extended to account for all EM field components in the near field region. Both far-field and near-field distributions have been obtained for s and p polarization (no depolarization takes place in this scattering geometry). We have presented far-field intensity distributions corresponding to single realizations (speckle patterns) and averages over an ensemble of realizations.

It has been shown that the details corresponding to scales below a hundred nanometers in moderately rough self-affine profiles produce no change in the far field speckle pattern, appearing only small quantitative variations for very large rms height. For p polarization, nonetheless, small changes are already observed for moderately rough profiles, becoming dramatic for large roughness. Ensemble averaging tends to wash out the differences. In the case of s polarization, the angular distributions of mean scattered intensities are practically identical, not only for $\delta = 51.45$ nm, but also for $\delta = 257$

nm. For p polarization, the differences encountered in the speckle patterns are largely suppressed in the mean scattered intensity distributions; the only effect of the varying nanoscale cutoff ξ_L manifests in the total reflectance (which is smaller for decreasing ξ_L due to larger absorption).

Nevertheless, nanoscale features have a strong impact on the near EM field distributions due to the relevant role played by the evanescent components. The s -polarized surface EM field intensity exhibits oscillations with higher frequency the smaller ξ_L is. The amplitude of such oscillations, and thus the changes from one profile to another with different ξ_L , increases with the rms height δ . No significant electric field enhancements are found in this polarization. Incidentally, the surface and near electric and magnetic field intensities vaguely resemble the surface profile with positive contrast despite the large surface roughness of the profiles. In the case of p polarization, drastic changes with decreasing ξ_L are found in the surface EM field stemming from the roughness-

induced excitation of SPP. Large, narrow peaks (*localized optical modes*) tend to appear with either increasing rms height or decreasing nanoscale, predominantly enhancing the normal electric field intensity (as expected from the SPP electric field orientation), and rapidly decaying into both vacuum and metal. Our near field intensity maps around optical excitations can help to interpret PSTM experimental results. In addition, the large field enhancements associated with such *localized optical modes* on self-affine fractal metal surfaces can shed light onto SERS and surface nonlinear optical phenomena.

Acknowledgments

This work was supported by the Spanish Dirección General de Investigación (grant BFM2000-0806) and Comunidad de Madrid (grant 07M/0111/2000).

-
- [1] B. B. Mandelbrot, *Fractals* (Freeman, San Francisco, 1977); *The Fractal Geometry of Nature* (Freeman, San Francisco, 1982).
- [2] J. Feder, *Fractals* (Plenum, New York, 1988).
- [3] A.-L. Barabási and H. E. Stanley, *Fractal Concepts in Surface Growth* (University Press, Cambridge, 1995).
- [4] M. V. Berry, "Diffractals," *J. Appl. Phys.* **12**, 781-797 (1979).
- [5] E. Jakeman, "Fraunhofer scattering by a sub-fractal diffuser," *Opt. Acta* **30**, 1207-1212 (1983).
- [6] D. L. Jaggard and Y. Kim, "Diffraction by band-limited fractal screens," *J. Opt. Soc. Am. A* **4**, 1055-1062 (1987); Y. Kim and D. L. Jaggard, "Optical beam propagation in a band-limited fractal medium," *J. Opt. Soc. Am. A* **5**, 1419-1426 (1988).
- [7] R. Jullien and R. Botet, "Geometrical optics in fractals," *Physica D* **38**, 208-212 (1989).
- [8] S. K. Sinha, "Scattering from fractal structures," *Physica D* **38**, 310-314 (1989).
- [9] B. J. West, "Sensing scaled scintillations," *J. Opt. Soc. Am. A* **7**, 1074-1100 (1990).
- [10] D. L. Jaggard and X. Sun, "Scattering from fractally corrugated surfaces," *J. Opt. Soc. Am. A* **7**, 1131-1139 (1990); "Fractal surface scattering: A generalized Rayleigh solution," *J. Appl. Phys.* **68**, 5456-5462 (1990).
- [11] H. N. Yang, T. M. Lu, and G. C. Wang, "Diffraction from surface growth fronts," *Phys. Rev. B* **47**, 3911-3922 (1993).
- [12] P. E. McSharry, P. J. Cullen, and D. Moroney, "Wave scattering by a two-dimensional band limited fractal surface based on a perturbation of the Green's function," *J. Appl. Phys.* **78**, 6940-6948 (1995).
- [13] N. Lin, H. P. Lee, S. P. Lim, and K. S. Lee, "Wave scattering from fractal surfaces," *J. Mod. Opt.* **42**, 225-241 (1995).
- [14] S. Savaidis, P. Frangos, D. L. Jaggard, and K. Hizanidis, "Scattering from fractally corrugated surfaces: an exact approach," *Opt. Lett.* **20**, 2357-2359 (1995); "Scattering from fractally corrugated surfaces with use of the extended boundary condition method," *J. Opt. Soc. Am. A* **14**, 475-485 (1997).
- [15] J. Chen, T. K. Y. Lo, H. Leung, and J. Litva, "The use of fractals for modeling EM wave scattering from rough sea surface," *IEEE Trans. Geosci.* **34**, 966-972 (1996).
- [16] C. J. R. Sheppard, "Scattering by fractal surfaces with an outer scale," *Opt. Commun.* **122**, 178-188 (1996).
- [17] A. Mendoza-Suárez and E. R. Méndez, "Light scattering by a reentrant fractal surface," *Appl. Opt.* **36**, 3521-3531 (1997).
- [18] J. A. Sánchez-Gil and J. V. García-Ramos, "Far-field intensity of electromagnetic waves scattered from random, self-affine fractal metal surfaces," *Waves in Random Media* **7**, 285-293 (1997).
- [19] I. Simonsen, A. Hansen, and O. M. Nes, "Determination of Hurst exponents by use of the wavelet transform," *Phys. Rev. E* **58**, 2779-2787 (1998).
- [20] Y.P. Zhao, G. C. Wang, and T. M. Lu, "Diffraction from non-Gaussian rough surfaces," *Phys. Rev. B* **55**, 13938-13952 (1997); Y.P. Zhao, C. F. Cheng, G. C. Wang, and T. M. Lu, "Power law behavior in diffraction from fractal surfaces," *Surf. Sci.* **409**, L703-L708 (1998).
- [21] G. Franceschetti, A. Iodice, and D. Riccio, "Scattering from dielectric random fractal surfaces via method of moments," *IEEE Trans. Geosci.* **38**, 1644-1655 (2000).
- [22] I. Simonsen, D. Vandembroucq, and S. Roux, "Wave scattering from self-affine surfaces," *Phys. Rev. E* **61**, 5914-5917 (2000); "Electromagnetic wave scattering from conducting self-affine surfaces: an analytic and numerical study," *J. Opt. Soc. Am. A* **18**, 1101-1111 (2001).
- [23] A. A. Maradudin, T. Michel, A. R. McGurn, and E. R. Méndez, "Enhanced backscattering of light from a random grating," *Ann. Phys. (New York)* **203**, 255-307 (1990).
- [24] M. Nieto-Vesperinas, *Scattering and Diffraction in Physical Optics* (Wiley, New York, 1991).
- [25] J. A. Sánchez-Gil and M. Nieto-Vesperinas, "Light scat-

- tering from random rough dielectric surfaces,” *J. Opt. Soc. Am. A* **8**, 1270-1286 (1991); “Resonance effects in multiple light scattering from statistically rough metallic surfaces,” *Phys. Rev. B* **45**, 8623-8633 (1992).
- [26] V. M. Shalaev, “Electromagnetic properties of small-particle composites,” *Phys. Rep.* **272**, 61-137 (1996).
- [27] E. Y. Poliakov, V. M. Shalaev, V. A. Markel, and R. Botet, “Enhanced Raman scattering from self-affine thin films,” *Opt. Lett.* **21**, 1628-1630 (1996).
- [28] J. A. Sánchez-Gil and J. V. García-Ramos, “Strong surface field enhancements in the scattering of p-polarized light from fractal metal surfaces,” *Opt. Commun.* **134**, 11-15 (1997).
- [29] J. A. Sánchez-Gil and J. V. García-Ramos, “Calculations of the direct electromagnetic enhancement in surface enhanced Raman scattering on random self-affine fractal metal surfaces,” *J. Chem. Phys.* **108**, 317-325 (1998).
- [30] E. Y. Poliakov, V. A. Markel, V. M. Shalaev, and R. Botet, “Nonlinear optical phenomena on rough surfaces of metal thin films,” *Phys. Rev. B* **57**, 14901-14913 (1998).
- [31] S. Grésillon, L. Aigouy, A. C. Boccara, J. C. Rivoal, X. Quelin, C. Desmaret, P. Gadenne, V. A. Shubin, A. K. Sarychev, and V. M. Shalaev, “Experimental observation of localized optical excitations in random metal-dielectric films,” *Phys. Rev. Lett.* **82**, 4520-4523 (1999).
- [32] J. A. Sánchez-Gil, J. V. García-Ramos, and E. R. Méndez, “Near-field electromagnetic wave scattering from random self-affine fractal metal surfaces: Spectral dependence of local field enhancements and their statistics in connection with surface-enhanced Raman scattering,” *Phys. Rev. B* **62**, 10515-10525 (2000).
- [33] D. P. Tsai, J. Kovacs, Z. Wang, M. Moskovits, V. M. Shalaev, J. S. Suh, and R. Botet, “Photon scanning tunneling microscopy images of optical excitations of fractal metal colloid clusters,” *Phys. Rev. Lett.* **72**, 4149-4152 (1994).
- [34] S. Bozhevolnyi, B. Vohnsen, I. I. Smolyaninov, and A. V. Zayats, “Direct observation of surface polariton localization caused by surface roughness,” *Opt. Commun.* **117**, 417-423 (1995).
- [35] S. Bozhevolnyi, B. Vohnsen, A. V. Zayats, and I. I. Smolyaninov, “Fractal surface characterization: implications for plasmon polariton scattering,” *Surf. Sci.* **356**, 268-274 (1996).
- [36] P. Zhang, T. L. Haslett, C. Douketis, and M. Moskovits, “Mode localization in self-affine fractal interfaces observed by near-field microscopy,” *Phys. Rev. B* **57**, 15513-15518 (1998).
- [37] S. Bozhevolnyi, V. A. Markel, V. Coello, W. Kim, and V. M. Shalaev, “Direct observation of localized dipolar excitations on rough nanostructured surfaces,” *Phys. Rev. B* **58**, 11441-11448 (1998).
- [38] V. A. Markel, V. M. Shalaev, P. Zhang, W. Huynh, L. Tay, T. L. Haslett, and M. Moskovits, “Near-field optical spectroscopy of individual surface-plasmon modes in colloid clusters,” *Phys. Rev. B* **59**, 10903-10909 (1999).
- [39] K. A. O’Donnell, R. Torre, and C. S. West, “Observations of backscattering effects in second-harmonic generation from a weakly rough metal surface,” *Opt. Lett.* **21**, 1738-1740 (1996); M. Leyva-Lucero, E. R. Méndez, T. A. Leskova, A. A. Maradudin, and J. Q. Lu, “Multiple-scattering effects in the second-harmonic generation of light in reflection from a randomly rough metal surface,” *Opt. Lett.* **21**, 1809-1811 (1996).
- [40] S. Nie and S. R. Emory, “Probing single molecules and single nanoparticles by surface-enhanced Raman scattering,” *Science* **275**, 1102-1106 (1997).
- [41] K. Kneipp, Y. Wang, H. Kneipp, L. T. Perlman, I. Itzkan, R. R. Dasari, and M. S. Feld, “Single molecule detection using surface-enhanced Raman scattering (SERS),” *Phys. Rev. Lett.* **78**, 1667-1670 (1997).
- [42] H. Xu, E. J. Bjerneld, M. Käll, and L. Börjesson, “Spectroscopy of single hemoglobin molecules by surface enhanced Raman scattering,” *Phys. Rev. Lett.* **83**, 4357-4360 (1999).
- [43] R. F. Voss, in *The Science of Fractal Images*, H.-O. Peitgen and D. Saupe, eds. (Springer, Berlin, 1988).
- [44] R. F. Voss, “Random fractals: Self-affinity in noise, mountains, and clouds,” *Physica D* **38**, 362-371 (1989).
- [45] D. W. Lynch and W. R. Hunter, in: *Handbook of Optical Constants of Solids*, edited by E. D. Palik (Academic Press, New York, 1985), p. 356.
- [46] R. Carminati and J. J. Greffet, “Influence of dielectric contrast and topography on the near field scattered by an inhomogeneous surface,” *J. Opt. Soc. Am. A* **12**, 2716-2725 (1995).
- [47] J. J. Greffet, A. Sentenac, and R. Carminati, “Surface profile reconstruction using near-field data,” *Opt. Commun.* **116**, 20-24 (1995).
- [48] J. A. Sánchez-Gil, J. V. García-Ramos, and E. R. Méndez, “Influence of nanoscale cutoff in random self-affine fractal silver surfaces on the excitation of localized optical modes,” *Opt. Lett.* **26**, 1286-1288 (2001).
- [49] E. Devaux, A. Dereux, E. Bourillot, J.-C. Weeber, Y. Lacroute, J.-P. Goudonnet, and C. Girard, “Local detection of the optical magnetic field in the near zone of dielectric samples,” *Phys. Rev. B* **62**, 10504-10514 (2000).

Figures

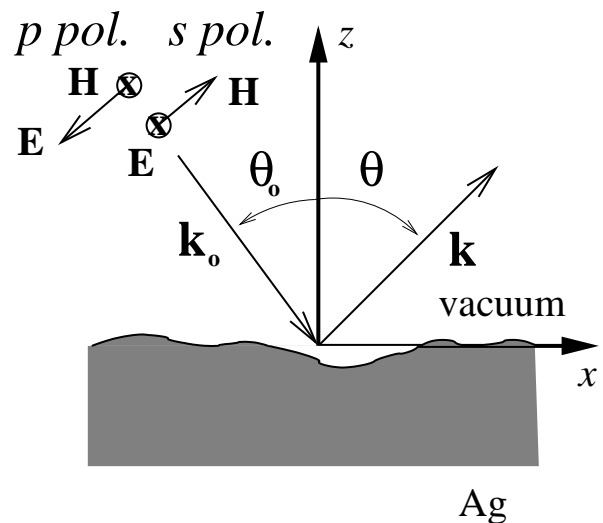


FIG. 1: Illustration of the scattering geometry.

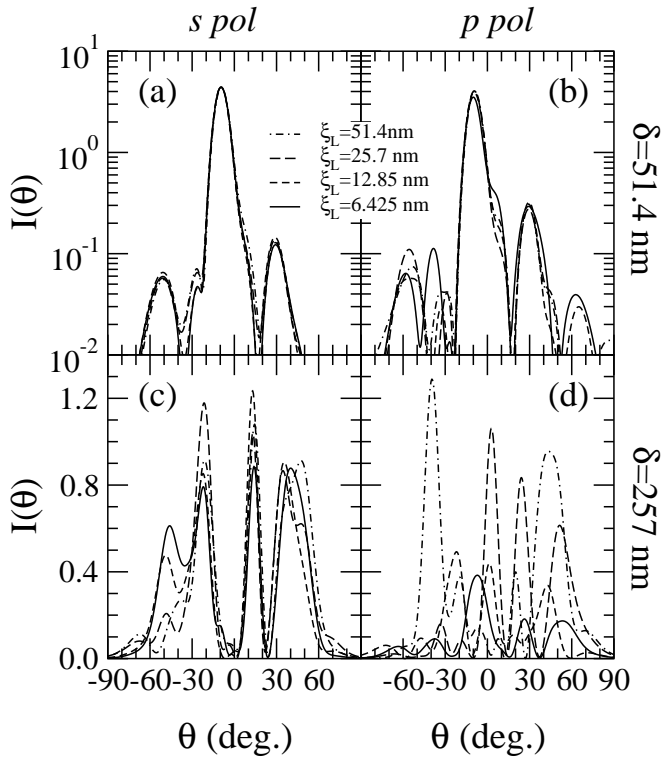


FIG. 2: Angular distribution of the speckle pattern intensity scattered from Ag fractal surface profiles with $L = 5.14 \mu\text{m}$, $D = 1.9$, and $\delta = 51.4 \text{ nm}$ (top, a-b) and $\delta = 257 \text{ nm}$ (bottom, c-d), differing only in $\xi_L = 51.4, 25.7, 12.85$, and 6.425 nm . illuminated by a Gaussian beam with $\theta_0 = -10^\circ$, $\lambda = 629.9 \text{ nm}$, and $W = L/4 \cos \theta_0$. Left (a and c): s polarization; right (b and d): p polarization.

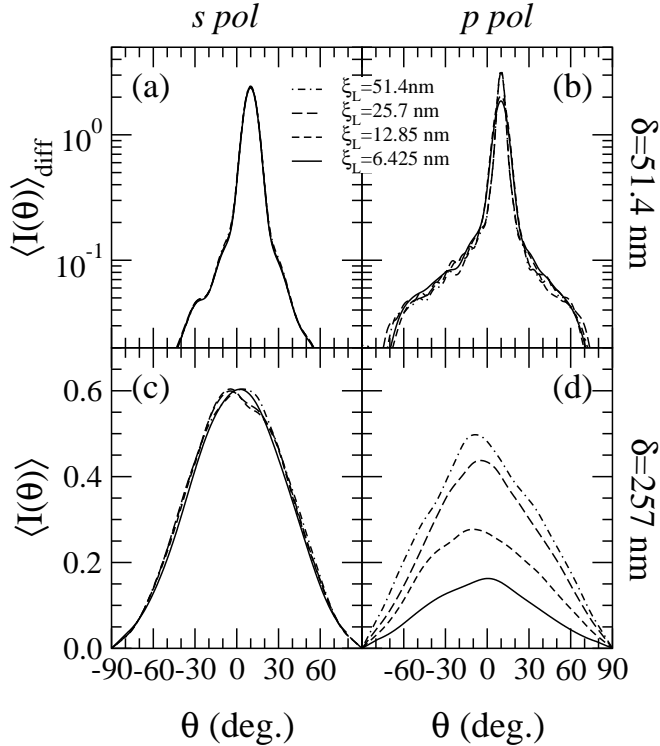


FIG. 3: Same as in Fig. 2 but for the mean scattered intensity averaged over $N_r = 200$ realizations.

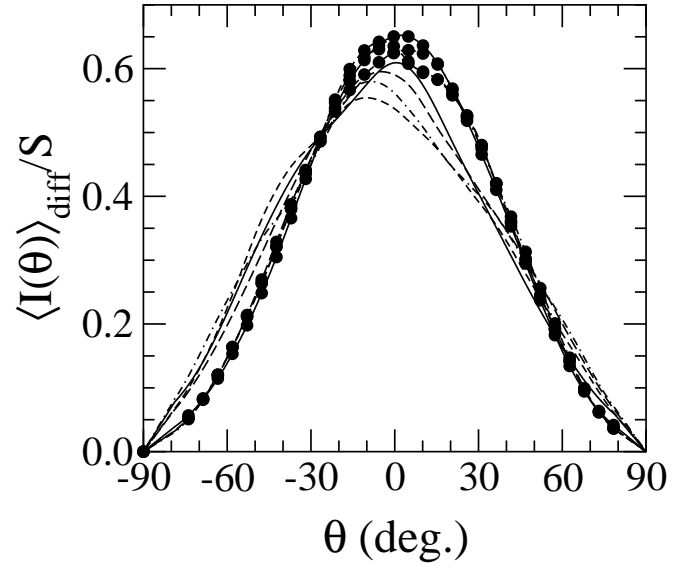


FIG. 4: Same as in Figs. 3c and 3d but renormalizing by the total reflectance S .

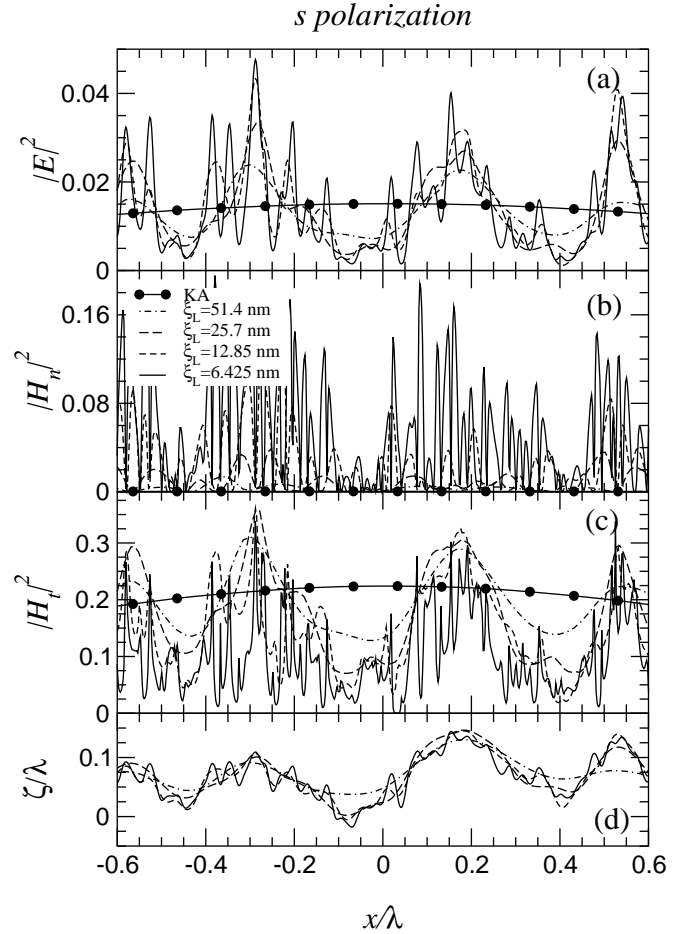


FIG. 5: Surface electric (a) and magnetic, normal (b) and tangential (c), field intensities on the center spot of the illuminated area $L = 5.14 \mu\text{m}$ for s -polarized scattering with $\theta_0 = -10^\circ$, $\lambda = 629.9 \text{ nm}$, and $W = L/4 \cos \theta_0$, from Ag fractal surfaces with $D = 1.9$, $\delta = 51.4 \text{ nm}$, and $\xi_L = 51.4, 25.7, 12.85,$ and 6.425 nm . The KA field intensity is also included (see text). (d) The corresponding surface profiles.

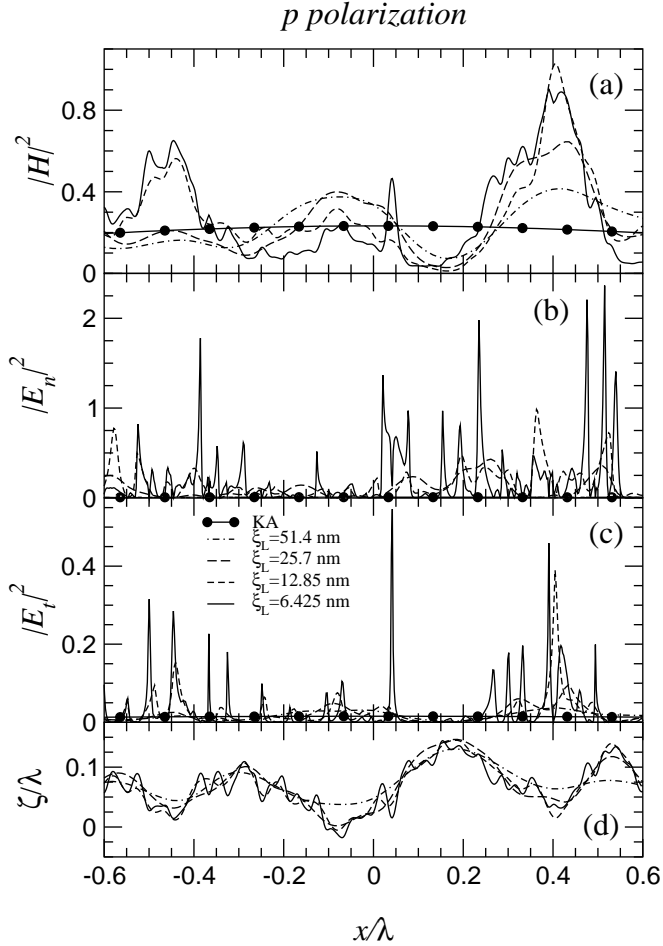


FIG. 6: Surface magnetic (a) and electric, normal (b) and tangential (c), field intensities on the center spot of the illuminated area $L = 5.14 \mu\text{m}$ for p -polarized scattering with $\theta_0 = -10^\circ$, $\lambda = 629.9 \text{ nm}$, and $W = L/4 \cos \theta_0$, from Ag fractal surfaces with $D = 1.9$, $\delta = 51.4 \text{ nm}$, and $\xi_L = 51.4, 25.7, 12.85,$ and 6.425 nm . The KA field intensity is also included (see text). (d) The corresponding surface profiles.

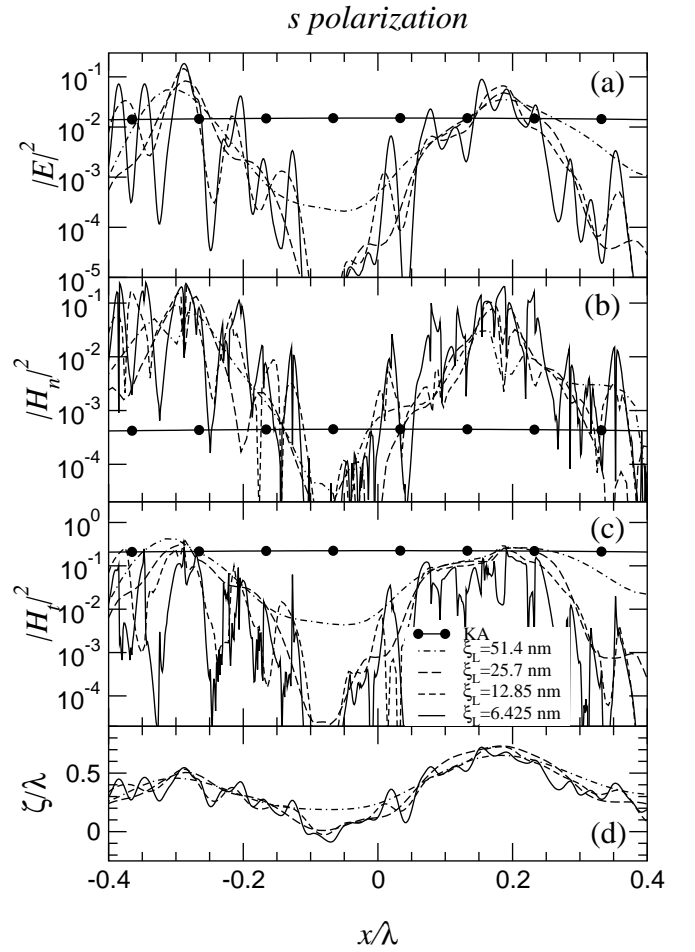


FIG. 7: Surface EM field intensities (in a semi-log₁₀ scale) for s polarization as in Fig. 5, but for rougher surface profiles (d) with $\delta = 257 \text{ nm}$.

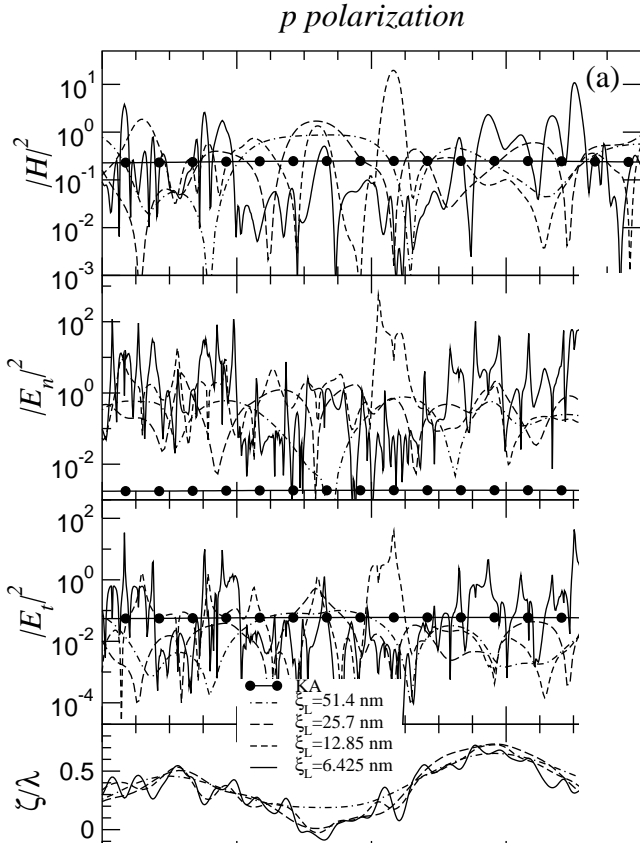


FIG. 9: Near field intensity images in *s* polarization [(a) electric, (b) magnetic, the former split into (c) *x*, horizontal component, and (d) *z*, vertical component, all of them in a \log_{10} scale] in an area of $0.5 \times 0.5 \mu\text{m}^2$ close to the fractal surface in Fig. 7d with $\delta = 257$ nm and $\xi_L = 12.85$ nm. Other parameters as in Fig. 7.

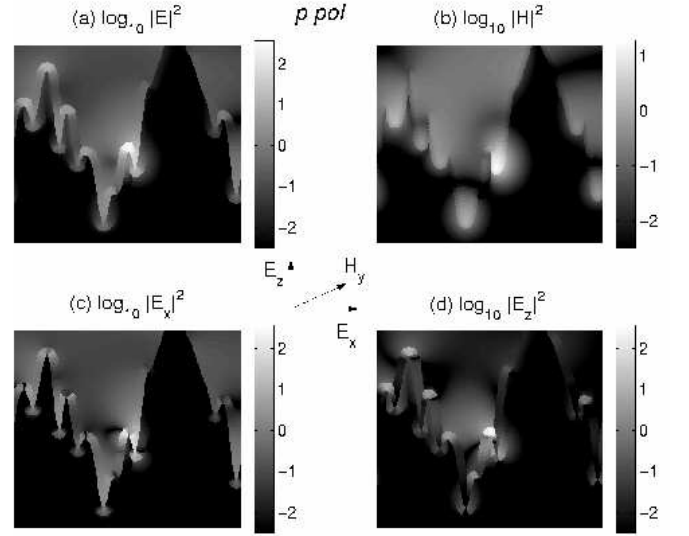


FIG. 10: Near field intensity images in *p* polarization [(a) electric, (b) magnetic, the latter split into (c) *x*, horizontal component, and (d) *z*, vertical component, all of them in a \log_{10} scale] in an area of $0.5 \times 0.5 \mu\text{m}^2$ close to the fractal surface in Fig. 8d with $\delta = 257$ nm and $\xi_L = 12.85$ nm, where a strong *localized optical mode* is observed. Other parameters as in Fig. 8.

